Synthesis and characterization of cationic iron complexes supported by the neutral ligands $NP^{i\text{-}Pr}_3$, $NArP^{i\text{-}Pr}_3$, and $NS^{t\text{-}Bu}_3$[1]

Cora E. MacBeth, Seth B. Harkins, and Jonas C. Peters

Abstract: This paper compares the local geometries, spin states, and redox properties of a series of iron complexes supported by neutral, tetradentate NP_3 (tris(phosphine)amine) and NS_3 (tris(thioether)amine) ligands. Our consideration of an Fe-mediated N_2 fixation scheme similar to that proposed by Chatt for molybdenum motivates our interest in systems of these types. This report specifically describes the synthesis and characterization of cationic Fe(II) chloride complexes supported by the neutral ligands $NP^{i\text{-}Pr}_3$ ($NP^{i\text{-}Pr}_3$ = $[N(CH_2CH_2P\text{-}i\text{-}Pr_2)_3]$), $NArP^{i\text{-}Pr}_3$ ($NArP^{i\text{-}Pr}_3$ = [N(2-diisopropylphosphine-4-methylphenyl)$_3$]), and $NS^{t\text{-}Bu}_3$ ($NS^{t\text{-}Bu}_3$ = $[N(CH_2CH_2S\text{-}t\text{-}Bu)_3]$). The solid-state structures, electrochemistry, and magnetic properties of these complexes are reported. Whereas the $NP^{i\text{-}Pr}_3$ and $NArP^{i\text{-}Pr}_3$ ligands provide pseudotetrahedral $S = 2$ ferrous cations $[Fe(NP^{i\text{-}Pr}_3)Cl]PF_6$ (**1**[PF_6]) and $[Fe(NArP^{i\text{-}Pr}_3)Cl]BPh_4$ (**2**[BPh_4]) featuring a long Fe—N bond distance, the $NS^{t\text{-}Bu}_3$ ligand gives rise to a trigonal bipyramidal structure with a $S = 1$ ground state and a much shorter Fe–N interaction. The complexes **1**[BPh_4] and **2**[BPh_4] can be reduced under CO to give rise to the five-coordinate Fe(I) monocarbonyls $[Fe(NP^{i\text{-}Pr}_3)CO]BPh_4$ (**4**[BPh_4]) and $[Fe(NArP^{i\text{-}Pr}_3)CO]BPh_4$ (**5**[BPh_4]). The solid-state structures and electrochemistry of **4**[BPh_4] and **5**[BPh_4] are described, as is the EPR spectrum of **4**[BPh_4]. The synthesis and characterization of the hydride–dinitrogen complex $[Fe(NP^{i\text{-}Pr}_3)(N_2)(H)]PF_6$ (**6**[PF_6]) has also been accomplished and its properties are also reported.

Key words: nitrogenase, iron, polydentate phosphines, thioether ligands, N_2 chemistry, nitrogen, Fe(I).

Résumé : Dans ce travail, on compare les géométries locales, états de spin et propriétés redox d'une série de complexes de fer supportés par les ligands neutres et tridentates NP_3 (tris(phosphine)amine) et NS_3 (tris(thioéther)amine). Notre considération d'un schéma de fixation du N_2 catalysé par le Fe semblable à celui proposé par Chatt pour le molybdène motive notre intérêt dans les systèmes de ce type. Dans ce travail, on décrit spécifiquement la synthèse et la caractérisation de complexes cationiques du chlorure de Fe(II) supportés par les ligands neutres $NP^{i\text{-}Pr}_3$ ($NP^{i\text{-}Pr}_3$ = $[N(CH_2CH_2P\text{-}i\text{-}Pr_2)_3]$), $NArP^{i\text{-}Pr}_3$ ($NArP^{i\text{-}Pr}_3$ = [N(2-diisopropylphosphine-4-méthylphényl)$_3$]) et $NS^{t\text{-}Bu}_3$ ($NS^{t\text{-}Bu}_3$ = $[N(CH_2CH_2S\text{-}t\text{-}Bu)_3]$), y compris les structures à l'état solide, l'électrochimie et les propriétés magnétiques de ces complexes. Alors que les ligands $NP^{i\text{-}Pr}_3$ et $NArP^{i\text{-}Pr}_3$ conduisent à des cations ferreux pseudotétraédriques $S = 2$ $[Fe(NP^{i\text{-}Pr}_3)Cl]PF_6$ (**1**[PF_6]) et $[Fe(NArP^{i\text{-}Pr}_3)Cl]BPh_4$ (**2**[BPh_4]) comportant une longue liaison Fe—N, le ligand $NS^{t\text{-}Bu}_3$ conduit à la formation d'un complexe de structure bipyramidale trigonale avec un état fondamental $S = 1$ et une interaction Fe–N beaucoup plus courte. Les complexes **1**[BPh_4] et **2**[BPh_4] peuvent être réduits sous l'influence du CO pour conduire à des complexes monocarbonylés et pentacoordinés du Fe(I), $[Fe(NP^{i\text{-}Pr}_3)CO]BPh_4$ (**4**[BPh_4]) et $[Fe(NArP^{i\text{-}Pr}_3)CO]BPh_4$ **5**[BPh_4]. On décrit aussi les structures solides et l'électrochimie des complexes **4**[BPh_4] et **5**[BPh_4] ainsi que le spectre RPE du composé **4**[BPh_4]. On a aussi réalisé la synthèse et la caractérisation du complexe hydrure–diazote $[Fe(NP^{i\text{-}Pr}_3)(N_2)(H)]PF_6$ (**6**[PF_6]) et on rapporte ses propriétés.

Mots clés : nitrogénase, fer, phosphines polydentates, ligands thioéther, chimie du N_2, azote, Fe(I).

[Traduit par la Rédaction]

Introduction

The site(s) of substrate binding and reactivity (e.g., N_2, HC≡CH, H^+, CO) at the inorganic cofactors of nitrogenase enzymes is a fascinating and complicated issue (1). Because crystallographic data is presently available only for the FeMo-nitrogenase (FeMo-N_2ase) enzyme (2), the biochemical (3), theoretical (4), and synthetic (1, 5), model communities have focused the bulk of their attention on understanding its mode of mechanistic action. The presence of a single molybdenum center in the FeMo-cofactor (2, 3*a*), in addition to a wealth of structurally diverse functional

Received 9 September 2004. Published on the NRC Research Press Web site at http://canjchem.nrc.ca on 23 March 2005.

C.E. MacBeth, S.B. Harkins, and J.C. Peters.[2] California Institute of Technology, Division of Chemistry and Chemical Engineering, Mail Code 127-72, 1200 E. California Blvd., Pasadena, CA 91125, USA.

[1]This article is part of a Special Issue dedicated to Dinitrogen Chemistry.
[2]Corresponding author (e-mail: jpeters@caltech.edu).

 doi: 10.1139/V05-017

Scheme 1.

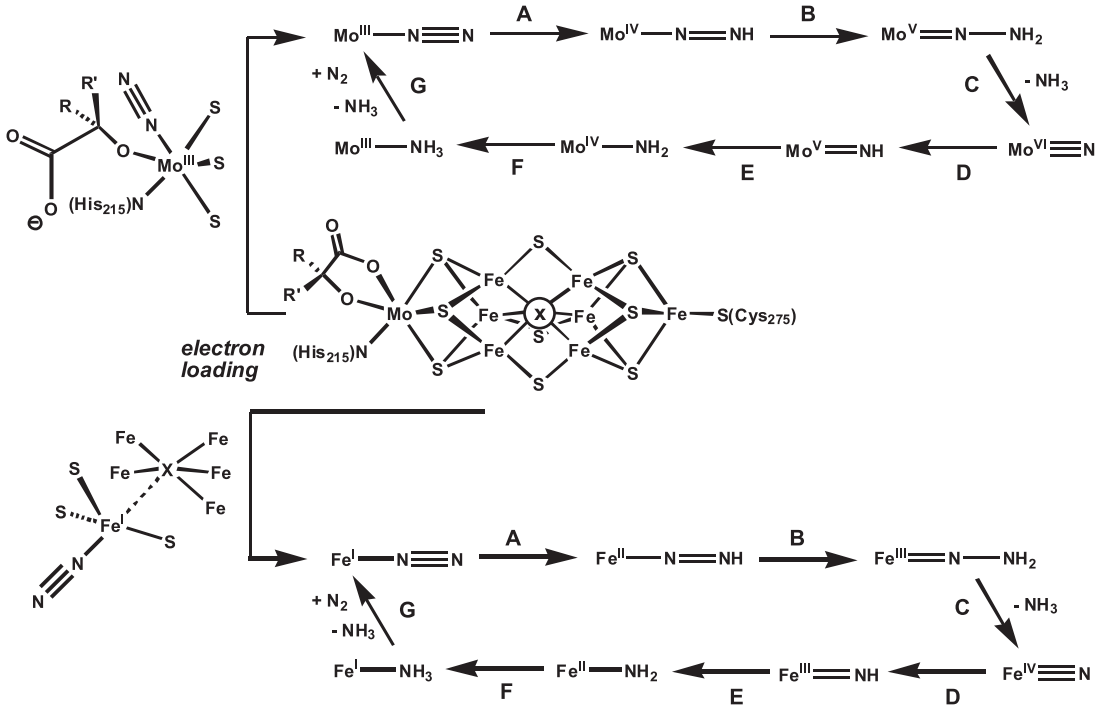

model systems (6), has reinforced the suggestion that a single molybdenum site may be responsible for mediating N_2 uptake and reduction in FeMo-N_2ase. Particularly attractive is a scheme akin to that originally put forward by Chatt et al. (7) and later modified by Pickett (8) in which a vacant Mo^{III} site, perhaps generated via homocitrate dechelation under electron loading conditions, binds N_2 to mediate its successive reduction to NH_3 by the successive transfer of protons and electrons. Such a scenario is schematically outlined in the top portion of Scheme 1. Significant in this regard is the recent work of Yandulov and Schrock (9), who have demonstrated that such a cycle can be accomplished in a small molecule synthetic system. They have shown that certain triamidoamine-supported molybdenum complexes are capable of catalytically shuttling among various oxidation states ($Mo^{III}/Mo^{IV}/Mo^{V}/Mo^{VI}$) as nitrogen is taken up and reduced to ammonia.

These successes not withstanding, it needs to be emphasized that iron is the only metal *known* to be ubiquitous to all nitrogenase enzymes (10) (also true of hydrogenase enzymes), and biochemical and spectroscopic data (11) are available to suggest that the iron sites of the FeMo-cofactor play a critical, albeit ill-defined, role in facilitating N_2 reduction, and myriad proposals have been put forth stressing an Fe-mediated N_2 fixation scheme. Problematic is that the inorganic dinitrogen chemistry of iron is far less well-developed than that for molybdenum, and therefore evaluating the chemical feasibility of such schemes is at present difficult. Most of the Fe-mediated scenarios being considered in the literature invoke multiple iron centers during N_2 uptake–reduction (5). This is due to the presence of multiple iron centers in the cofactor, and perhaps more importantly, to the implicit assumption that a single iron site cannot support the various N_x intermediates, oxidation states, and multi-electron transformations that would need to be invoked *en route* to NH_3 production from N_2 (bottom of Scheme 1, steps A–G), in sharp contrast to the case of redox-rich molybdenum.

Inorganic coordination chemistry can play a key role with respect to expanding our understanding of the N_2 chemistry available to iron, and in testing the validity of the assumptions mentioned above. The recent structural assignment of a central light atom in the MoFe-cofactor core (2) suggests that, if one or more iron atoms in the central section of the cofactor provides an initial site for N_2 uptake (3*a*), then coordinatively unsaturated iron centers provide plausible starting points for inorganic iron model chemistry (12). At the bottom of Scheme 1 we sketch a N_2 reduction scenario that mirrors that of the molybdenum postulate, but in this case invokes a hemi-labile role for the central light atom that exposes a low-valent iron site for N_2 uptake under electron loading conditions. Such a scenario would set the stage for the further reduction of N_2 to ammonia, perhaps via a Chatt-type cycle based upon iron (steps A–G). Fe–N_x model complexes will help to evaluate the chemical feasibility of this mechanistic scheme. Depending on the degree to which the Fe–X linkage is broken during the cycle, four- and (or) five-coordinate complexes may be considered as the most appropriate starting points.

In this context, our own group has recently developed four-coordinate iron, phosphine-supported systems of the generic type $L_3Fe–N_x$ (13). These pseudotetrahedral platforms exhibit: (*i*) an unprecedented degree of redox flexibility for mononuclear iron systems; (*ii*) a fascinating propensity to populate low-spin, ground-state configurations for pseudotetrahedral Fe^{2+}, Fe^{3+}, and Fe^{4+} species; and (*iii*) a capacity to accommodate strongly π-basic (e.g., N^{3-}, NR^{2-}), π-acidic (e.g., N_2), and intermediate type (e.g., N_2R^-, NR_2^-) ligands

Scheme 2.

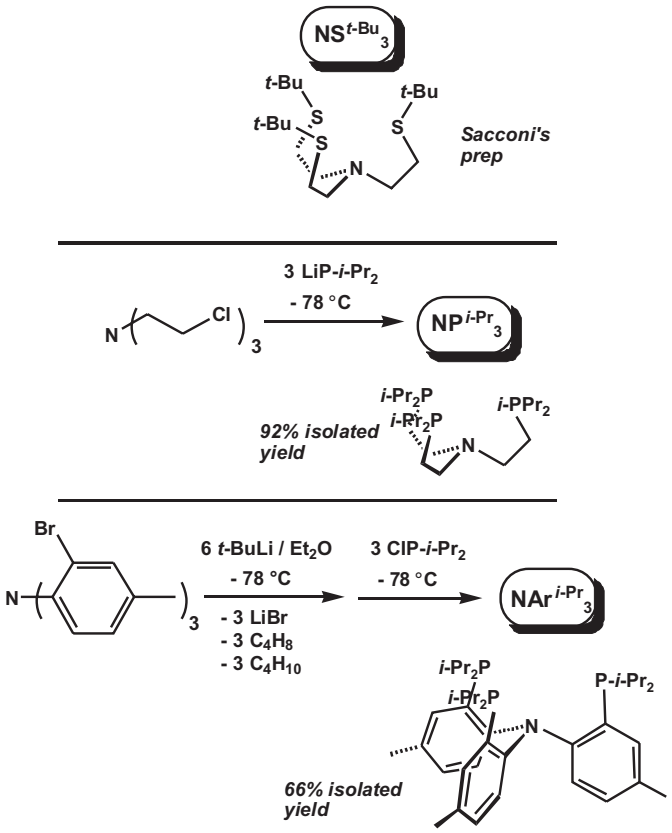

Scheme 3.

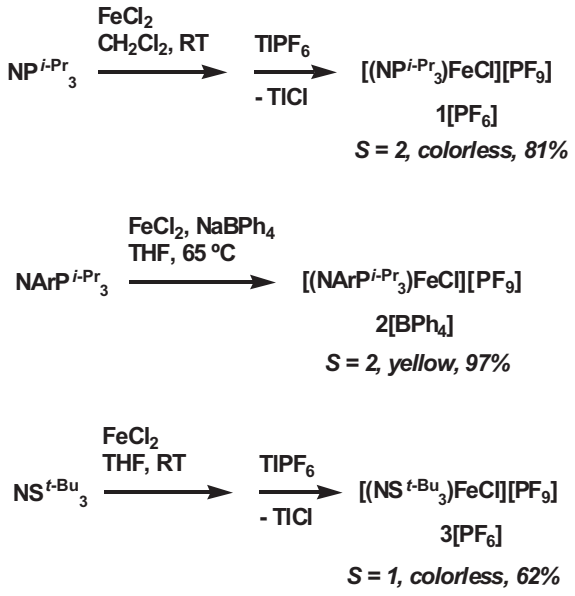

at a single coordination site. An obvious question that emerges is whether five-coordinate iron scaffolds will display similar properties.

In the present paper, we compare the local geometries, spin states, and redox properties of a series of iron complexes supported by neutral, tetradentate NP_3 (tris(phosphine)amine) and NS_3 (tris(thioether)amine) ligands (14). Two new NP_3-type ligands are introduced, $NP^{i\text{-Pr}}_3$ ($NP^{i\text{-Pr}}_3$ = $N(CH_2CH_2P\text{-}i\text{-}Pr_2)_3$) and $NArP^{i\text{-Pr}}_3$ ($NArP^{i\text{-Pr}}_3$ = N(2-diisopropylphosphine-4-methylphenyl)$_3$) are described, and we establish the nature of their ferrous "$(NP_3)Fe^{II}$–X" ions. For comparison, we also describe a structurally related "$(NS^{t\text{-Bu}}_3)Fe^{II}$–X" system ($NS^{t\text{-Bu}}_3$ = (e.g., $N(CH_2CH_2S\text{-}t\text{-}Bu)_3$)) (14). It is established that the $NP^{i\text{-Pr}}_3$ and $NArP^{i\text{-Pr}}_3$ scaffolds support unusual monovalent, trigonal bipyramidal monocarbonyl derivatives. Additionally, it is demonstrated that the $NP^{i\text{-Pr}}_3$ ligand supports N_2 coordination to iron.

Results and discussion

Five-coordinate iron complexes supported by neutral, tetradentate NP_3 (15, 16) and PP_3 (17) ligands are well-known, dating back to the early pioneering efforts of Sacconi and co-workers (14, 15). Despite the general utility of these types of polydentate phosphines, little attention has been paid to derivatives with sterically encumbering phosphine substituents. To begin to explore such systems we have targeted the preparation of the isopropyl-substituted systems $NP^{i\text{-Pr}}_3$ and $NArP^{i\text{-Pr}}_3$ (Scheme 2). Isopropyl-substituted $NP^{i\text{-Pr}}_3$ can be prepared by a straightforward modification of the literature procedure for NP^{Ph}_3 (NP^{Ph}_3 = $N(CH_2CH_2PPh_2)_3$) (14). Accordingly, the addition of 3 equiv. of lithium diisopropylphosphide to an ethereal solution of tris(2-chloroethyl)amine at low temperature affords $NArP^{i\text{-Pr}}_3$ in excellent isolated yield (92%) following work-up. Preparation of $NArP^{i\text{-Pr}}_3$ requires a combination of a suitable carbanion nucleophile and chlorophosphine electrophile. We find that the addition of chlorodiisopropylphosphine to an ethereal solution of $[2\text{-Li-4-Me-}C_6H_3]_3N$, generated in situ by the addition of *tert*-butyllithium to tris(*o*-bromo-*p*-tolyl)amine, affords crystalline $NArP^{i\text{-Pr}}_3$ in good yield (66%) after work-up.

As shown in Scheme 3, cationic Fe(II)–chloride complexes of these NP_3-type ligands can be prepared by reacting the neutral phosphine ligands with $FeCl_2$ in the presence of a halide abstraction reagent ($TlPF_6$ or $NaBPh_4$) in either CH_2Cl_2 or THF, providing colorless $[Fe(NP^{i\text{-Pr}}_3)Cl]PF_6$ (**1**[PF_6]) and yellow $[Fe(NArP^{i\text{-Pr}}_3)Cl]BPh_4$ (**2**[BPh_4]). For structural and magnetic comparison, we also prepared the colorless complex $[Fe(NS^{t\text{-Bu}}_3)Cl]PF_6$ (**3**[PF_6]) by the addition of $FeCl_2$ to a THF solution of $NS^{t\text{-Bu}}_3$ followed by chloride abstraction with $TlPF_6$. The isolated yield of **3**[PF_6] is fairly good (62%), although not in comparison to the high yields obtained for **1**[PF_6] and **2**[BPh_4]. Somewhat surprising is that the iron chemistry of Sacconi's $NS^{t\text{-Bu}}_3$ ligand has not been previously described, though its coordination to the first row transition metals Co (18), Ni (19), and Cu (20) has been known for some time. Given the sulfur-rich environment of the central iron sites of the MoFe-cofactor, and the possible presence of an interstitial N atom, $NS^{t\text{-Bu}}_3$ and related ligands provide an interesting structural starting point for functional iron model studies.

X-ray diffraction analyses of single crystals of **1**[PF_6], **2**[BPh_4], and **3**[PF_6] (Fig. 1) establishes that each complex is monomeric. NP_3-supported **1**[PF_6] and **2**[BPh_4] are best described as tetrahedral complexes and are structurally quite similar to the ferrous cation of NP^{Ph}_3 (15*b*). Accordingly, **1**[PF_6] features an elongated Fe-N distance of 2.801(3) Å

Fig. 1. Displacement ellipsoid (50%) representation of **1**[PF_6], **2**[BPh_4], and **3**[PF_6]. Hydrogen atoms and counteranions have been removed for clarity. Selected bond lengths (Å) and angles (°) for **1**[PF_6]: Fe—Cl 2.262(2), Fe—P1 2.455(1), Fe—N 2.801(3), N-Fe-Cl 180.00(11), P1-Fe-P′ 112.10(2), P1-Fe-Cl 106.70(2). For **2**[BPh_4]: Fe—Cl 2.253(2), Fe—P1 2.467(2), Fe—P2 2.485(2), Fe—P3 2.481(2), Fe—N 2.701(2), P1-Fe-C1 103.83(6), P2-Fe-Cl 115.89(5), P3-Fe-Cl 105.64(4), Fe-N 2.701(2). For **3**[PF_6]: Fe—Cl 2.298(1), Fe—S1 2.447(1), Fe—S2 2.453(1), Fe—S3 2.407(1), Fe—N 2.378(3), N-Fe-Cl 178.32(8), S1-Fe-Cl 101.38(4), S2-Fe-Cl 97.54(4), S3-Fe-Cl 100.11(4).

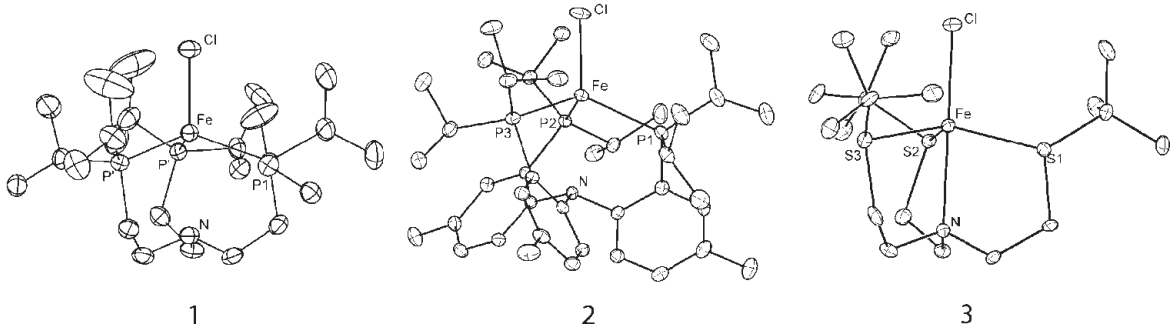

1 2 3

(2.701(2) Å for **2**[BPh_4]) (21). The iron centers in **1**[PF_6] and **2**[BPh_4] lie above the P_3 plane, projected into the hemisphere opposite the apical N atom. Both systems are high spin (S = 2), expected for conventional pseudotetrahedral iron(II) systems.

It is interesting that the local geometry of sulfur-supported **3**[PF_6] is better described as trigonal bipyramidal. It displays a much shorter Fe–N interaction (2.378(3) Å), which in turn places the Fe center closer to the plane created by its three sulfur donor atoms. The trigonal bipyramidal geometry of **3**[PF_6] gives rise to an average S-Fe-Cl bond angle of 99.7°. For comparison, the average P-Fe-Cl angles of **1**[PF_6] and **2**[BPh_4] are 106.7° and 108.5°, respectively, closer to that expected for an idealized tetrahedral geometry (109.5°). The fact that complex **3**[PF_6] adopts a higher coordination number is perhaps reflective of the decreased electron-releasing character of sulfur relative to phosphorus, resulting in a more electron-deficient iron center that draws the additional N-atom donor inward. The spin state of **3**[PF_6] (S = 1) also reflects the change in coordination number. Two unpaired electrons are expected for an σ-only *d*-orbital splitting scheme under a trigonal bipyramidal ligand field.

Electrochemical characterization of **1**[PF_6] and **2**[BPh_4] shows that each system supports a reversible $Fe^{II/I}$ redox process (–1.65 V for **1**[PF_6] and –1.51 V for **2**[BPh_4]; internally referenced to Cp_2Fe in THF). Only **1**[PF_6] affords a reversible $Fe^{III/II}$ couple (0.54 V). Cationic **2**[BPh_4] is irreversibly oxidized at above ca. 0.5 V. For comparison, we note that NS_3-supported **3**[PF_6] does not feature any well-defined redox processes in the potential window scanned, although problematic adsorption of the complex to the glassy carbon electrode cannot be discounted. Electrochemical data for **1**[PF_6] and **2**[BPh_4] suggests that Fe(I) species should be accessible, at least for the phosphine-supported complexes. While the neutral iron(I) chloride complexes of $NP^{i\text{-}Pr}{}_3$ and $NArP^{i\text{-}Pr}{}_3$ have proven synthetically elusive, formal replacement of the chloride by CO leads to well-defined cationic iron(I) species. Thus, tetraphenylborate salts of $\mathbf{1}^+$ and $\mathbf{2}^+$ can be reduced by Na/Hg amalgam in THF under a blanket of CO to provide deep red, crystalline material. Thorough analysis establishes the products to be the cationic, monocarbonyl derivatives [$Fe(NP^{i\text{-}Pr}{}_3)CO$]$BPh_4$ (**4**[BPh_4]) and [$Fe(NArP^{i\text{-}Pr}{}_3)CO$]$BPh_4$ (**5**[BPh_4]), each of which is isolated in high yield (>85%). Attempts to prepare the related iron(I) $NS^{t\text{-}Bu}{}_3Fe(CO)^+$ species by similar strategies have not been successful.

Structurally characterized, Fe(I) monocarbonyl complexes are rare. To our knowledge, Parkin and co-workers (22) have reported the only crystallographically characterized example of such a species, which is pseudotetrahedral, using an anionic substituted tris(pyrazolyl)borate ligand auxiliary. Recently, we have reported the structural characterization of an iron(I) dicarbonyl complex, which is approximately square pyramidal, supported by an anionic tris(phosphino)borate ligand (13*a*). The solid-state structures of **4**[BPh_4] and **5**[BPh_4] were obtained for comparison and are shown in Fig. 2. Each cationic complex is rigorously trigonal bipyramidal. The Fe—N bond distances observed for **4**[BPh_4] (2.150(2) Å) and **5**[BPh_4] (2.164(2) Å) are dramatically contracted (>0.6 Å) compared with their Fe(II)–chloride precursors. Each carbonyl derivative also displays an unusually short Fe—C bond length (1.680(4) Å for **4**[BPh_4], 1.709(2) Å for **5**[BPh_4]) because of the presence of very strong π backbonding from the iron(I) centers into the π* orbitals of the coordinated CO ligand. The strength of this interaction is also reflected by the observation of very low ν(CO) stretching frequencies (1881 cm^{-1} for **4**[BPh_4], 1880 cm^{-1} for **5**[BPh_4]; THF/KBr). For comparison, Parkin's four-coordinate iron(I) monocarbonyl [$PhTp^{t\text{-}Bu}$]Fe(CO) exhibits a longer Fe—C bond length of 1.789(3) Å, and a ν(CO) value of 1907 cm^{-1} (22). Despite their cationic nature, the π-backbonding ability of **4**[BPh_4] and **5**[BPh_4] is appreciably stronger than in Parkin's tetrahedral derivative, presumably resulting from the presence of a fifth donor group.

The cyclic voltammetry of complexes **4**[BPh_4] and **5**[BPh_4] was also studied. As shown in Fig. 3, both species exhibit two fully reversible redox processes that we assign as $Fe^{I/0}$ (–1.6 V for **4**[BPh_4] and **5**[BPh_4]) and $Fe^{II/I}$ (–0.3 V for **4**[BPh_4], –0.2 V for **5**[BPh_4]) redox events. Bianchini et al. (23) have explored the cyclic voltammetry of a related iron system, [$(PP_3)Fe(C{\equiv}CPh)$]BPh_4, which shows a reversible $Fe^{II/I}$ process but an irreversible $Fe^{I/0}$ event. The neutral π-acidic CO ligand of $\mathbf{4}^+$ and $\mathbf{5}^+$ is better able to stabilize the zero-valent state of iron than the anionic phenylacetylide ligand of [$(PP_3)Fe(C{\equiv}CPh)$]BPh_4.

Because complexes **4**[BPh_4] and **5**[BPh_4] represent rather

Fig. 2. Displacement ellipsoids (50%) of **4**[BPh_4], **5**[BPh_4], and **6**[PF_6]. Hydrogen atoms and counteranions have been removed for clarity. Selected bond lengths (Å) and angles(°) for **4**[BPh_4]: Fe—C 1.680(4), Fe—N 2.150(2), Fe—P1 2.2939(8), Fe—P2 2.2379(8), Fe—P3 2.2851(8), C-Fe-N 177.43(11). For **5**[BPh_4]: Fe—C 1.709(3), Fe—N 2.164(2), Fe—P1 2.3091(7), Fe—P2 2.2936(7), Fe—P3 2.2722(7), C-Fe-N 177.6(1). For **6**[PF_6]: Fe—N2 1.804(3), Fe—N1 2.142(3), Fe—H 1.53(4), Fe—P1 2.245(1), Fe—P2 2.250(1), Fe—P3 2.286(1), N1-Fe-N2 176.4(1).

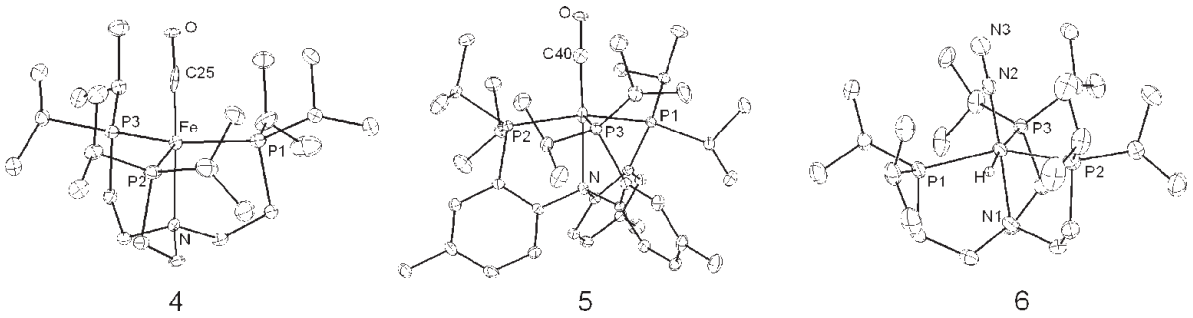

Fig. 3. Cyclic voltammograms of **5**[BPh_4] and **4**[BPh_4] recorded at 100 mV/s in THF vs. $Ag/AgNO_3$.

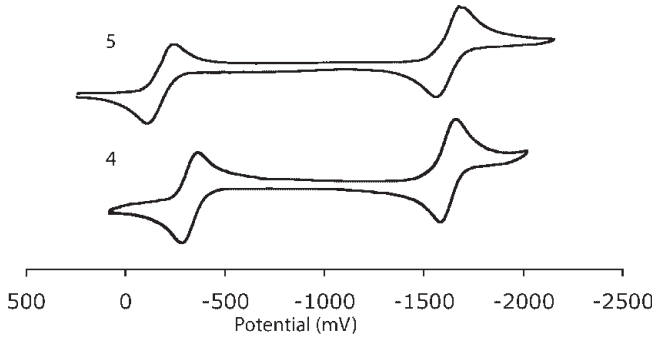

Fig. 4. EPR spectrum of **4**[BPh_4] (5.4 K, ν = 9.475 GHz) recorded in a frozen glass of 1-methyltetrahydrofuran. (A) Experimental spectrum, (B) simulated spectrum: g_1 = 2.302, $a_{1(P)}$ = 30 G; g_2 = 2.0365, $a_{2(P)}$ = 15 G; g_3 = 2.0075, $a_{3(P)}$ = 28 G.

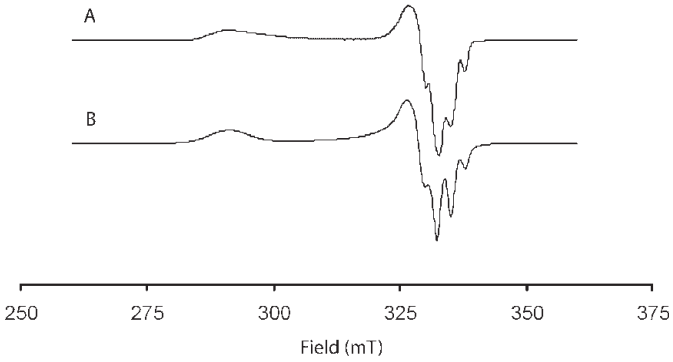

unusual examples of mononuclear iron(I) carbonyls it was prudent to undertake their magnetic characterization. Solution moments for **4**[BPh_4] and **5**[BPh_4] (24, d_8-THF) were measured to be 2.05 μ_B and 1.96 μ_B, respectively, implying a doublet ground state for each species. We also collected a glassy 1-methyltetrahydrofuran EPR spectrum of **4**[BPh_4] at 5.4 K (Fig. 4A). The observed signal, which is rhombic with three components at g_1 = 2.3020, g_2 = 2.0365, and g_3 = 2.0075, shows well-resolved superhyperfine coupling to the phosphorus nuclei of the ligand (3 × P, I_p = 1/2). The spectrum can be satisfactorily simulated as an S = 1/2 spin system by inclusion of the superhyperfine interactions (Fig. 4B). The three-component, rhombic signal observed is qualitatively comparable to that reported by Bianchini et al. (23) for the iron(I) derivative (PP_3)Fe(C≡CPh). However, Bianchini notes the absence of superhyperfine interactions between the unpaired electron and the phosphorous nuclei of PP_3 as a result of a spin-spin exchange narrowing processes occurring at sufficiently fast rates. The presence of resolvable superhyperfine interactions in the spectrum of **4**[BPh_4] likely benefits from the acquisition of the spectrum in the glassy phase.

The reduction of the cationic complexes **1**, **2**, and **3** under dinitrogen is a topic of ongoing study. For the present contribution, we note that N_2 uptake can be achieved by the ($NP^{i\text{-}Pr}_3$)Fe system by slight modification of the route used for the original preparation of [(NP^{Ph}_3)Fe(H)(N_2)][BPh_4] (NP^{Ph}_3 = $N(CH_2CH_2PPh_2)_3$) (15*a*, 16). Addition of a THF solution of Li[BEt_3H] to **1**[PF_6] under N_2 generates yellow, diamagnetic [Fe($NP^{i\text{-}Pr}_3$)(N_2)(H)]PF_6 (**6**[PF_6]) in good yield. Complex **6**[PF_6] has been thoroughly characterized and its X-ray crystal structure is shown in Fig. 2. The spectroscopic and structural data for **6**[PF_6] compare favorably with those reported for [(NP^{Ph}_3)Fe(H)(N_2)][BPh_4] (16). The ν(N_2) vibration is observed at only slightly lower energy for **6**[PF_6] (2087 vs. 2090 cm^{-1} in THF/KBr), and the Fe—N_{N2} bond distances are indistinguishable (1.81(1) Å). The ν(Fe-H) vibration for **6**[PF_6], which has been confirmed by preparation of a deuterated sample, is shifted to a much lower frequency than for [(NP^{Ph}_3)Fe(H)(N_2)][BPh_4] (1865 vs. 1913 cm^{-1}), likely reflecting the presence of an isopropyl-substituted rather than a phenyl-substituted phosphine donor trans to the hydride.

In conclusion, we have attempted to motivate renewed interest in the small molecule coordination chemistry of five-coordinate iron systems supported by ligands that allow access to low-valent states. Understanding potential reactivity patterns for local iron sites of the cofactor of nitrogenase provides one such impetus. In this regard, we have expanded the versatile NP_3 ligand set popularized by Sacconi and co-workers (15) to include the bulkier, more electron-releasing $NArP^{i\text{-}Pr}_3$ and $NP^{i\text{-}Pr}_3$ derivatives that feature isopropyl-substituted phosphine donors. The iron coordination chemistry of these new generation polyphosphine ligands is well-defined, and iron(I) carbonyl and iron(II)

dinitrogen adducts have been described. A key feature of these tetradentate ligands concerns the flexibility of the ligand. The apical Fe–N donor interaction reacts to the nature of the ligand in the fifth binding site: it contracts for π-acidic CO (Fe(I) relative to chloride (Fe(II)). The related but less electron-releasing $NS^{t\text{-}Bu}_3$ ligand supports a well-defined, cationic $(NS_3)Fe^{II}$–Cl species whose local geometry and donor ligands are interesting given the local geometry of the central iron sites of the MoFe-cofactor of nitrogenase. A difference in spin state is observed when comparing the $(NS^{t\text{-}Bu}_3)Fe^{II}$–Cl complex **3**[$PF_6$] ($S = 1$) and its $(NP_3)Fe^{II}$–Cl analogues ($S = 2$). This difference results from a severe contraction of the apical Fe–N linkage to lend a trigonal bipyramidal rather than a tetrahedral geometry for the divalent iron center in **3**[PF_6]. Future work will examine the installation of nitrogenous donor ligands in the fifth binding site of these scaffolds.[3]

Experimental section

All manipulations were carried out using standard Schlenk or glovebox techniques under a nitrogen atmosphere. All solvents were deoxygenated and dried by sparging with N_2 gas and passage through an activated alumina column. Non-halogenated solvents were tested with a standard purple solution of sodium benzophenone ketyl in tetrahydrofuran to ensure dioxygen and water removal. Deuterated solvents were purchased from Cambridge Isotopes Laboratories, Inc. and were degassed and stored over activated 3 Å molecular sieves prior to use. All other reagents and solvents were purchased from commercial vendors and used without further purification unless otherwise noted. $NS^{t\text{-}Bu}_3$ (14), LiP-*i*-Pr_2 (25), and $N(CH_2CH_2Cl)_3$ (26) were prepared according to literature procedures. *CAUTION: $N(CH_2CH_2Cl)_3$ (a mustard agent) and thallium reagents are toxic and should be handled with extreme care.*

Elemental analyses were performed by Desert Analytics, Tucson, Arizona. A Varian Mercury-300 spectrometer was used to record ^1H and ^{31}P NMR spectra at room temperature. ^1H and ^{13}C NMR chemical shifts were referenced to residual solvent. ^{31}P NMR are reported relative to an external standard of 85% H_3PO_4 (0 ppm). Abbreviations for reported signal multiplicites are as follows: singlet (s), doublet (d), triplet (t), quartet (q), multiplet (m), broad (br). IR spectra were recorded on a Bio-Rad Excalibur FTS 3000 spectrometer controlled by Win-IR Pro software using a KBr solution cell. MS data were obtained by injection of a hydrocarbon solution onto a Hewlett-Packard 1100MSD mass spectrometer (ES^+) or an Agilent 5973 mass selective detector (EI). UV–vis measurements were recorded on a Varian Cary 50 Bio spectrophotometer controlled by Cary WinUV Software. All measurements were recorded using a quartz cell fitted with a Teflon® cap.

Room temperature solution magnetic susceptibilities were determined using the method of Evans (24). Electrochemical measurements were recorded in a glovebox under a dinitrogen atmosphere using a BAS CV 100 W (Bioanalytical Systems Inc., West Lafayette, Indiana). A glassy carbon working electrode, a platinum wire auxiliary electrode, and a $Ag/AgNO_3$ nonaqueous reference electrode were used in all studies. All measurements were carried out in THF solutions of electrolyte (0.32 mol/L tetra-*n*-butylammonium hexafluorophosphate) and analyte. All electrochemical measurements are referenced to Fc/Fc^+ as an internal standard.

X-band EPR measurements were recorded using a Bruker EMX spectrometer (controlled by Bruker Win EPR software version 3.0) equipped with a rectangular cavity working in the TE_{102} mode. Low-temperature measurements were conducted with an Oxford continuous-flow helium cryostat. Accurate frequency values were recorded from a frequency counter on the microwave bridge. Solution spectra were acquired in 1-methyltetrahydrofuran. Samples were prepared in a glovebox under dinitrogen in a quartz EPR tube equipped with a ground glass joint.

Crystallographic data for complexes **1**–**6** appear in Tables 1 and 2. X-ray diffraction studies were carried out at the Beckman Institute Crystallographic Facility on a Bruker Smart 1000 CCD diffractometer. Crystals were mounted on a glass fiber with Paratone-N oil. Crystallographic data were collected on a Bruker P4 diffractometer (0.710 73 Å MoKα) with a CCD area detector. Data were collected using the Bruker SMART program, collecting scans at five settings. Data reduction was performed using Bruker SAINT v6.2. Structure solution and structure refinement were performed using SHELXS-97 (Sheldrick, 1990) and SHELXL-97 (Sheldrick, 1997).

Refinement of F^2 against all reflections

The weighted *R* factor (*wR*) and goodness of fit (S) are based on F^2, conventional *R* factors (*R*) are based on *F*, with *F* set to zero for negative F^2. The threshold expression of $F^2 > 2\sigma(F^2)$ is used only for calculating *R* factors(gt), etc., and is not relevant to the choice of reflections for refinement. *R* factors based on F^2 are statistically about twice as large as those based on *F*, and *R* factors based on *all* data will be even larger.

All esds (except the esd in the dihedral angle between two l.s. planes) are estimated using the full covariance matrix. The cell esds are taken into account individually in the estimation of esds in distances, angles, and torsion angles; correlations between esds in cell parameters are only used when they are defined by crystal symmetry. An approximate (isotropic) treatment of cell esds is used for estimating esds involving l.

Synthesis of $NP^{i\text{-}Pr}_3$

In a 100 mL flask, tris(2-chloroethyl)amine (1.72 g, 8.41 mmol) was dissolved in THF (100 mL) and cooled to –78 °C, while stirring, for 30 min. Diisopropyllithiophosphine (3.34 g, 26.9 mmol) was dissolved in THF (50 mL)

[3] Supplementary data may be purchased from the Directory of Unpublished Data, Document Delivery, CISTI, National Research Council Canada, Ottawa, ON K1A 0S2, Canada (http://cisti-icist.nrc-cnrc.gc.ca/irm/unpub_e.shtml for information on ordering electronically). CCDC 261768–261770 and 240830–240832 contain the crystallographic data for this manuscript. These data can be obtained, free of charge, via ww.ccdc.cam.ac.uk/conts/retrieving.html (or from the Cambridge Crystallographic Data Centre, 12 Union Road, Cambridge CB2 1EZ, UK; fax +44 1223 336033; or deposit@ccdc.cam.ac.uk).

Table 1. Crystallographic data and detail of refinement for **1**[PF_6], **2**[BPh_4], and **3**[PF_6].

Crystal	[Fe(NP$^{i\text{-Pr}}_3$)Cl]PF_6	[Fe(NArP$^{i\text{-Pr}}_3$)Cl]BPh_4	[Fe(NS$^{t\text{-Bu}}_3$)Cl]PF_6
Empirical formula	$C_{24}H_{54}NP_4ClF_6Fe$	$C_{63}H_{80}BClFeNP_3$	$C_{18}H_{39}NPS_3ClF_6Fe$
Formula weight	685.86	1046.30	601.95
Crystal system	Cubic	Triclinic	Monoclinic
Space group	$P2_13$	P-1 (No. 2)	$P2_1/n$
a (Å)	14.8923(8)	10.992(9)	16.7388(15)
b (Å)		14.940(12)	12.0505(11)
c (Å)		17.893(15)	27.017(3)
α (°)		83.95(3)	
β (°)		79.03(3)	101.593(2)
γ (°)		89.11(3)	
V (Å^3)	3 302.8(3)	2 869(4)	5 338.4(8)
Z	4	2	8
D_{calcd} (Mg/m^3)	1.379	1.211	1.498
Radiation (MoKα)	λ = 0.710 73 Å	λ = 0.710 73 Å	λ = 0.710 73 Å
T (K)	100(2)	100(2)	100(2)
θ Range (°)	2.36–29.47	1.37–34.70	1.86–31.49
Total reflections	43 333	70 110	52 733
Unique reflections	3 511	21 858	15 469
Parameters	116	646	605
R_1, w$R2$ ($I > 2\sigma(I)$)[a]	0.045, 0.072	0.0452, 0.0836	0.0595, 0.0977
Goodness-of-fit on F^2	2.594	1.236	1.460

[a] $R_1 = \Sigma||F_o| - |F_c|| / \Sigma|F_o|$; $wR2 = \{\Sigma[w(F_o^2 - F_c^2)^2] / \Sigma[w(F_o^2)^2]\}^{1/2}$.

Table 2. Crystallographic data and detail of refinement for **4**[BPh_4], **5**[BPh_4], and **6**[PF_6].

Crystal	[Fe(NP$^{i\text{-Pr}}_3$)CO]BPh_4	[Fe(NArP$^{i\text{-Pr}}_3$)CO]BPh_4·THF	[Fe(NP$^{i\text{-Pr}}_3$)N_2(H)]PF_6
Empirical formula	$C_{48}H_{74}BNOP_3Fe$	$C_{64}H_{80}BFeNOP_3$·C_4H_8O	$C_{24}H_{55}F_6FeN_3P_4$
Formula weight	852.66	1110.96	679.44
Crystal system	Monoclinic	Monoclinic	Triclinic
Space group	$P2_1/c$	P 1 21/c 1 (No. 14)	P-1
a (Å)	17.4370(9)	11.1069(6)	9.9335(9)
b (Å)	11.3322(6)	22.6213(13)	11.2697(10)
c (Å)	24.3169(13)	23.9289(14)	14.8239(14)
α (°)			99.275(2)
β (°)	104.5680(10)°	91.349(2)	97.251(2)
γ (°)			95.764(2)
V (Å^3)	4 650.5(4)	6 010.5(6)	1 612.3(3)
Z	4	4	2
D_{calcd} (Mg/m^3)	1.218	1.228	1.400
Radiation (MoKα, Å)	λ = 0.710 73	λ = 0.710 73	λ = 0.710 73
T (K)	100(2)	100(2)	100(2)
θ Range (°)	1.73–28.43	1.70–33.81	1.9–32.7
Total reflections	61 863	102 345	52 733
Unique reflections	11 004	21 841	8 000
Parameters	517	700	378
R_1, w$R2$ ($I > 2\sigma(I)$)[a]	0.0626, 0.0988	0.0678, 0.1397	0.0604, 0.1519
Goodness-of-fit on F^2	2.206	1.006	1.09

[a] $R_1 = \Sigma||F_o| - |F_c|| / \Sigma|F_o|$; $wR2 = \{\Sigma[w(F_o^2 - F_c^2)^2] / \Sigma[w(F_o^2)^2]\}^{1/2}$.

and added dropwise to the stirring, cold solution of tris(2-chloroethyl)amine over the course of 30 min. After addition of the diisopropyllithiophosphine was complete, the reaction was slowly warmed to room temperature and stirred for 3 h. All volatiles were removed in vacuo to yield a pale yellow oil and white precipitate. The reaction mixture was then stirred in diethylether (30 mL) for 20 min. The resulting mixture was then filtered through a 60 mL, medium porosity, scintered glass frit that was layered with 1 inch (1 inch = 25.4 mm) of Celite® and 1 inch (1 inch = 25.4 mm) of silica gel. The white solids collected on the frit where then washed with two 20 mL portions of petroleum ether. All volatiles

were removed from the filtrate to yield $NP^{i\text{-}Pr}_3$ as a very viscous, pale yellow oil (3.48 g, 92%). ^{1}H NMR (300 MHz, C_6D_6): 2.87 (dt, 5.4 Hz, 6H), 1.5–1.75 (m, 12H) 1.05 (m, 36H). ^{13}C NMR (75 MHz, C_6D_6): 53.2 (d, 29.5 Hz), 24.1 (d, 14.3 Hz), 20.6 (t, 16.6 Hz), 19.4 (d, 9.7 Hz). ^{31}P NMR (121.4 MHz, C_6D_6): 0.78 (br s). FAB-MS (*m*/*z*): 450.3526 ($NP^{i\text{-}Pr}_3$ + H^+).

Synthesis of $NArP^{i\text{-}Pr}_3$

In a 100 mL flask, tris(2-bromo-*p*-tolyl)amine (3.0 g, 5.73 mmol) was dissolved in ether (50 mL) and cooled to –78 °C. Solid *t*-BuLi (2.2 g, 34.4 mmol) was added portionwise over 15 min. The reaction was warmed to room temperature after 30 min. Following 3 h of stirring, the reaction mixture was yellow in color with LiBr precipitate. The reaction vessel was cooled to –78 °C and chlorodiisopropylphosphine (2.8 g, 18.0 mmol) was added over 5 min. The mixture was stirred at ambient temperature for 18 h at which time it was filtered through a plug of silica gel and the solvent removed in vacuo. The resulting tacky solid was dissolved in CH_2Cl_2 (50 mL), filtered through Celite®, and dried to a solid. Trituration of the filtrate in methanol (150 mL) afforded an analytically pure fine white solid, which was collected on a fritted glass funnel and dried thoroughly under reduced pressure (2.4 g, 66%). ^{1}H NMR (300 MHz, $CDCl_3$): 7.25 (s), 7.16 (br s), 6.95 (s), 6.93 (s), 6.87 (dd, 2.0 Hz, 8.0H), 6.48 (dd, 4.0 Hz, 8.0H), 2.54 (m), 2.30 (s), 2.28 (s), 1.51 (d sept, 2.0 Hz, 7.0H), 1.21 (q, 7.5 Hz, 14.5H), 1.13 (dd, 7.0 Hz, 10.0H), 1.00 (br s), 0.91 (dd, 7.5 Hz, 10.0H), 0.825 (br s), 0.41 (7.5 Hz, 14H). ^{13}C NMR (126 MHz, $CDCl_3$): 155.1 (m), 154.5 (m), 135.0 (m), 134.7 (s), 133.9 (br s), 131.9 (s), 129.9 (br s), 129.3 (s), 127.7 (s), 23.9 (m), 23.4 (m), 21.9 (m), 21.1 (s), 21.0 (s), 19.2 (m). ^{31}P NMR (121 MHz, $CDCl_3$): –2.87 (br m), –11.28 (s). Anal. calcd. for $C_{39}H_{60}NP_3$: C 73.67, H 9.51, N 2.20; found: C 73.57, H 9.25, N 2.05.

Synthesis of $[Fe(NP^{i\text{-}Pr}_3)Cl]PF_6$ (1[PF_6])

Solid $FeCl_2$ (0.335 g, 2.65 mmol) was added to a stirring solution of $NP^{i\text{-}Pr}_3$ (1.19 g, 2.56 mmol) dissolved in CH_2Cl_2 (2.0 mL). The slurry was stirred for 10 min and $TlPF_6$ was added dropwise as a THF (4.0 mL) solution over 15 min. A white precipitate began to form immediately. The reaction was stirred for 4 h and then filtered through Celite®. The pad of Celite® was washed with two portions of CH_2Cl_2 (5.0 mL). All volatiles were then removed in vacuo to yield a white solid. The white solid was extracted into CH_2Cl_2 (5.0 mL) and again filtered through a pad of Celite®. The colorless solution was then layered with Et_2O and stored at –35 °C for 2 days to afford colorless crystals of the desired product (1.48 g, 81.3%). μ_{eff} (CD_2Cl_2, 298 K): 5.04 μ_B. ^{1}H NMR (300 MHz, CD_2Cl_2): 27.5 (b), 3.2 (b), –8.5 (b). ^{31}P NMR (121.4 MHz, CD_2Cl_2): –141.5 (septet, 711 Hz, PF_6). Anal calcd. for $C_{24}H_{54}ClF_6FeNP_4$: C 42.03, H 7.94, N 2.04; found: C 42.13, H 8.00, N 2.05.

Synthesis of $[Fe(NP^{i\text{-}Pr}_3)Cl]BPh_4$ (1[BPh_4])

The tetraphenylborate salt was synthesized in a similar maner as **1**, with the following exceptions: sodium tetraphenylborate was used in place of $TlPF_6$, and methanol was used in place of THF.

Synthesis of $[Fe(NArP^{i\text{-}Pr}_3)Cl]BPh_4$ (2[BPh_4])

A 50 mL reaction vessel was charged with $NArP^{i\text{-}Pr}_3$ (1.0 g, 1.57 mmol), $FeCl_2$ (0.20 g, 1.57 mmol), sodium tetraphenylborate (0.540 g, 1.57 mmol), and THF (25 mL) and sealed with a Teflon® stopper. The reaction was heated at 65 °C for 12 h, cooled, and the solvent was removed in vacuo. The resultant yellow solids were washed with petroleum ether (2 × 20 mL) and dried under reduced pressure. The product was extracted into CH_2Cl_2, filtered through a plug of Celite® and layered petroleum ether, which afforded analytically pure yellow crystals upon standing (1.60 g, 97%). Crystals suitable for X-ray diffraction were obtained by layering an CH_2Cl_2 solution with diethylether. μ_{eff} (acetone-d_6, 298 K): 5.3 μ_B. ^{1}H NMR (300 MHz, CD_2Cl_2): 140.9 (br s), 30.2 (br s), 19.4 (br s), 15.3 (s), 15.0 (s), 9.76 (s), 7.32 (s), 7.03 (t, 7.8 Hz), 6.87 (m), 5.03 (s), –3.05 (br s), –16.1 (br s), –20.7 (br s). Anal. calcd. for $C_{63}H_{80}BClFeNP_3$: C 72.32, H 7.71, N 1.34; found: C 72.08, H 7.53, N 1.46.

Synthesis of $[Fe(NS^{t\text{-}Bu}_3)Cl]PF_6$ (3[PF_6])

$NS^{t\text{-}Bu}_3$ (0.133 g, 0.364 mmol) was stirred in 5.0 mL of THF and solid $FeCl_2$ (0.0457 g, 0.364 mmol) was added. A THF solution (4.0 mL) of $TlPF_6$ (0.127 g, 0.364 mmol) was added to the reaction dropwise over 20 min. A white precipitate began to form immediately. The reaction mixture was stirred for 3 h, concentrated to dryness, dissolved in CH_2Cl_2 (3.0 mL), and filtered through a pad of Celite®. Layering the resulting colorless filtrate with Et_2O produced colorless crystals (0.136 g, 62%) of the desired product. ^{1}H NMR (300 MHz, d_8 -THF): 20.5 (b), 10.9 (b), 2.6 (b). ^{31}P NMR (121.4 MHz, THF-d_8): –143.5 (septet, 711 Hz, PF_6). Anal. calcd. for $C_{18}H_{39}ClF_6FeNP$: C 35.91, H 6.16, N 2.33; found: C 35.23, H 6.16, N 2.46.

Synthesis of $[Fe(NP^{i\text{-}Pr}_3)(CO)]BPh_4$ (4[BPh_4])

A 0.23 weight% amalgam was prepared in a 25.0 mL Shlenk flask by dissolving solid Na (5.1 mg, 0.22 mmol) in mercury (2.21 g). The flask was then charged with $[Fe(NP^{i\text{-}Pr}_3)Cl]BPh_4$ (0.190 g, 0.221 mmol) dissolved in THF (5.0 mL) and a stir bar. The headspace of the flask was quickly evacuated and refilled three times with 1 atm of CO(g) (1 atm = 101.325 kPa). After the third cycle, the flask was sealed under 1 atm of CO(g) (1 atm = 101.325 kPa) and stirring commenced. The reaction mixture changed immediately from colorless to bright yellow. The reaction mixture was stirred for 12 h over which the color changed again from golden yellow to dark red. All volatiles were removed in vacuo and the resulting red-brown solid was extracted into THF (3.0 mL) and filtered through a pad of Celite® to remove insoluble material. The resulting red solution was layered with Et_2O and stored at –35 °C overnight. The next day, large red crystals of the product were isolated on a medium porosity frit and dried. IR (THF, KBr, cm^{-1}) ν(CO): 1881. μ_{eff} (THF-d_8, 298 K): 2.15 μ_B. ^{1}H NMR (THF-d_8): 19.1 (b), 7.65 (b), 7.2 (b), 7.0 (b), 3.6 (b), –0.47 (b). Anal. calcd. for $C_{49}H_{75}BFeNOP_4$: C 68.94, H 8.86, N 1.64; found: C 68.96, H 8.62, N 1.66.

Synthesis of $[Fe(NArP^{i\text{-}Pr}_3)(CO)]BPh_4$ (5[BPh_4])

In a 50 mL Schlenk flask, $[(NArP^{i\text{-}Pr}_3)FeCl][BPh_4]$ (60 mg, 0.057 mmol) was dissolved in THF (50 mL) and so-

dium metal (1.3 mg, 0.057 mmol) amalgamated in mercury (1.84 g, 9.17 mmol) was added. The solution was sparged with CO(g) for 10 min and then stirred vigorously for 18 h during which time the solution became green in color. The solvent was removed under reduced pressure, and the resultant green solids were extracted with THF (5 mL) and then filtered. The green filtrate was layered with petroleum ether (15 mL) and the desired product precipitated as analytically pure red crystals (49 mg, 83%). μ_{eff} (THF-d_8, 298 K): 2.1 μ_B. IR (THF, KBr, cm^{-1}) ν(CO): 1880. Anal. calcd. for $C_{63}H_{80}BFeNOP_3$: C 73.99, H 7.76, N 1.35; found: C 73.76, H 7.70, N 1.47.

Synthesis of $[Fe(NP^{i\text{-}Pr}{}_3)(N_2)(H)]PF_6$ (6[PF_6])

Solid **1**[PF_6] (0.222 g, 0.324 mmol) was dissolved in THF (10 mL) and cooled to –78 °C. To this solution a solution of $Li(HBEt_3)$ (1.0 mol/L in ether) (356 μL, 0.356 mmol) was added dropwise via syringe. The reaction mixture changed slowly from colorless to pale yellow over 1 h. The reaction mixture was warmed to room temperature and filtered through a pad of Celite®. The yellow filtrate was dried in vacuo to yield a yellow-brown solid. The solid was extracted into THF (4.0 mL) and filtered through a pad of Celite®. The filtrate was layered with Et_2O (4.0 mL) and stored at –35 °C for 3 days to afford light yellow crystals of the desired product (0.142 g, 66%). IR (THF, KBr, cm^{-1}): ν(N_2) 2090, ν(FeH) 1865. ^{1}H NMR (300 MHz, THF-d_8): –8.77 (dt, J_{PH} = 74.1 Hz (cis), J_{PH} = 38.1 Hz (trans)), 1.4–1.6 (m, 36H), 1.8 (t, 2H), 1.94 (m, 4H), 1.98 (m, 2H), 2.15–2.25 (m, 4H), 2.32 (m, 2H), 2.48 (m, 2H) 2.70 (m, 2H). ^{31}P NMR (121.4 MHz, THF-d_8): 67.6 (d, 2P J_{pp}= 41.4 Hz), 62.2 (t, 1P), –141.5 (septet, 1P, J_{FP} = 711 Hz, PF_6). Anal. calcd. for $C_{24}H_{55}F_6FeN_3P_4$: C 42.43, H 8.16, N 6.18; found: C 42.82, H 8.16, N 5.72.

Synthesis of $[Fe(NP^{i\text{-}Pr}{}_3)(N_2)(D)]PF_6$

$Fe(NP^{i\text{-}Pr}{}_3)(N_2)(D)]PF_6$ was prepared by following the synthetic protocol outlined for **6**[PF_6] and using $Li(DBEt_3)$ in place of $Li(HBEt_3)$. The IR (THF, KBr) for this complex exhibits a ν(FeD) = 1341 cm^{-1}.

Acknowledgement

We acknowledge the DOE (Department of Energy) (PECASE), the NSF (National Science Foundation) (CHE-0132216), and the Beckman Institute Senior Research Fellows Program (CEM) for financial support. Larry Henling and Dr. Michael Day provided crystallographic assistance.

References

1. (*a*) S.C. Lee and R.H. Holm. Proc. Natl. Acad. Sci. U.S.A. **100**, 3595 (2003); (*b*) P.L. Holland. *In* Comprehensive coordination chemistry 2. Vol. 8. *Edited by* J.A. McLeverty and T.J. Meyer. Elsevier, New York. 2003. pp. 569–599.
2. O. Einsle, F.A. Tezcan, S.L.A. Andrade, B. Schmid, M. Yoshida, J.B. Howard, and D.C. Rees. Science, **297**, 1696 (2002).
3. (*a*) L.S. Seefeldt, I.G. Dance, and D.R. Dean. Biochemistry, **43**, 1401 (2004); (*b*) B.K. Burgess and K.J. Lowe. Chem. Rev. **96**, 2983 (1996).
4. (*a*) V. Vrajmasu, E. Münch, and E.L. Bominaar. Inorg. Chem. **42**, 5974 (2003); (*b*) H. Uwe, R. Ahlrichs, and D. Coucouvanis. J. Am. Chem. Soc. **126**, 2588 (2004).
5. (*a*) D. Coucouvanis, J. Han, and N. Moon. J. Am. Chem. Soc. **124**, 216 (2002); (*b*) J. Vela, S. Stoian, C.J. Flashenriem, E. Münck, and P.L. Holland. J. Am. Chem. Soc. **126**, 4522 (2004).
6. (*a*) J. Chatt, J.R. Dilworth, and R.L. Richards. **78**, 589 (1978); (*b*) F. Barriere. Coord. Chem. Rev. **236**, 71 (2003).
7. J. Chatt, J.R. Dilworth, and R.L. Richards. Chem. Rev. **78**, 589 (1978).
8. C.J. Pickett. J. Biol. Inorg. Chem. **1**, 601 (1996).
9. D.V. Yandulov and R.R. Schrock. Science, **301**, 76 (2003).
10. J.B. Howard and D.C. Rees. Chem. Rev. **96**, 2965 (1996).
11. H. Lee, R.Y. Igarashi, M. Laryukhin, P.E. Doan, P.C. Dos Santos, D.R. Dean, L.C. Seefeldt, and B.M. Hoffman. J. Am. Chem. Soc. **126**, 9563 (2004).
12. J.M. Smith, R.J. Lachicotte, K.A. Pittard, T.R. Cundari, G. Lukat-Rodgers, K.R. Rodgers, and P.L. Holland. J. Am. Chem. Soc. **123**, 9222 (2001).
13. (*a*) S.D. Brown, T.A. Betley, and J.C. Peters. J. Am. Chem. Soc. **125**, 322 (2003); (*b*) T.A. Betley and J.C. Peters. J. Am. Chem. Soc. **125**, 10 782 (2003); (*c*) T.A. Betley and J.C. Peters. J. Am. Chem. Soc. **126**, 6252 (2004).
14. R. Morassi and L. Sacconi. Inorg. Synth. **16**, 174 (1976).
15. (*a*) P. Stoppioni, F. Mani, and L. Sacconi. Inorg. Chim. Acta, **11**, 227 (1974); (*b*) L. Sacconi and M.D. Vaira. Inorg. Chem. **17**, 810 (1978); (*c*) M. Di Vaira, C.A. Ghilardi, and L. Sacconi. Inorg. Chem. **15**, 1555 (1976); (*d*) M. Di Vaira, S. Minollini, and L. Sacconi. Inorg. Chem. **16**, 1518 (1977).
16. T.A. George, D.J. Rose, and Y. Chang, Q. Chen, J. Zubieta. Inorg. Chem. **34**, 1295 (1995).
17. For examples see: (*a*) C. Bianchini, A. Meli, M. Peruzzini, C. Bohanna, M.A. Esteruelas, and L.A. Oro. Organometallics, **11**, 138 (1992); (*b*) L.D. Field, B.A. Messerle, and R.J. Smernik. Inorg. Chem. **36**, 5984 (1997); (*c*) L.D. Field, B.A. Messerle, R.J. Smernik, T.W. Hambley, and P. Turner. Inorg. Chem. **36**, 2884 (1997).
18. G. Fallani, R. Morassi, and F. Zanobini. Inorg. Chim. Acta, **12**, 147 (1975).
19. (*a*) P. Stavropoulos, M. Carrie, M.C. Muetterties, and R.H. Holm. J. Am. Chem. Soc. **112**, 5385 (1990); (*b*) P. Stavropoulos, M.C. Muetterties, M. Carrie, and R.H. Holm. J. Am. Chem. Soc. **113**, 8485 (1991).
20. (*a*) J.M. Baumeister, R. Alberto, K. Ortner, and O.B. Spingler. J. Chem. Soc. Dalton Trans. 4143 (2002); (*b*) E.A. Ambundo, A.J. Grall, N. Aguera-Vega, L.T. Dressel, T.H. Cooper, M.J. Heeg, L.A. Ochrymowyc, and D.B. Rorabacher. Inorg. Chem. **38**, 4233 (1999).
21. Long M-N distances are often observed for $[(NP_3)M(II)–X]^+$ complexes. See for example: (*a*) C.A. Ghilardi, C. Mealli, S. Midollini, and A. Orlandini. Inorg. Chem. **24**, 164 (1985); (*b*) M. Di Vaira and A.B. Orlandini. Inorg. Chem. **12**, 1292 (1973).
22. J.L. Kisko, T. Hascall, and G. Parkin. J. Am. Chem. Soc. **120**, 10 561 (1998).
23. C. Bianchini, F. Laschi, D. Masi, F.M. Ottavini, A. Pastor, M. Peruzzini, P. Zanello, and F. Zanobini. J. Am. Chem. Soc. **115**, 2723 (1993).
24. (*a*) S.K. Sur. J. Magn. Reson. **82**, 169 (1989); (*b*) D.F. Evans. J. Chem. Soc. 2003 (1959).
25. (*a*) A.H. Cowely, R.H. Jones, M.A. Mardones, and C.M. Nunn. Organometallics, **10**, 1635 (1991); (*b*) K. Issleib and F. Krech. J. Organomet. Chem. **13**, 283 (1968).
26. J.P. Mason and D.J. Gasch. J. Am. Chem. Soc. **60**, 2816 (1938).